Available online at www.sciencedirect.com
ScienceDirect
Advances in Space Research 46 (2010) 1024–1031
ADVANCES IN SPACE RESEARCH (a COSPAR publication)
www.elsevier.com/locate/asr

Evaluation of global modeling of M(3000)F2 and hmF2 based on alternative empirical orthogonal function expansions

Man-Lian Zhang *, Chunxu Liu, Weixing Wan, Libo Liu, Baiqi Ning

Beijing National Observatory of Space Environment, Institute of Geology and Geophysics, Chinese Academy of Sciences, Beijing 100029, China

Received 21 September 2009; received in revised form 9 October 2009; accepted 14 October 2009

Abstract

Global modeling of M(3000)F2 and hmF2 based on three alternative EOF (empirical orthogonal function) expansion methods is described briefly. Data used for the model construction is the monthly median hourly values of M(3000)F2 from the ionosonde/digisonde stations distributed around the world for the period of 1975–1985 and the hmF2 data of the same period converted from the measured M(3000)F2 based on the strong anti-correlation existing between them. Independent data of a low (1965) and a high (1970) solar activity year are used to validate the three alternative models based on different EOF expansion methods. Comparisons between the modeled results and observed data for both the low (1965) and high (1970) solar activity years showed good agreement for both M(3000)F2 and hmF2 parameters. Statistical analysis on the differences between model values and observed data showed that all the three alternative models (Model A, B and C) based on the different EOF expansion methods have better agreement with the observed data than the models currently used in IRI. All three alternative EOF based models have almost the same accuracy. Discussion on the preference of the three alternative EOF based models is given.

Keywords: Ionospheric models; M(3000)F2/hmF2; EOF analysis; F2 peak parameters; Global modeling

1. Introduction

Many empirical ionospheric models such as the International Reference Ionosphere (IRI) (Bilitza, 1990, 2001) and NeQuick (Leitinger et al., 2005) use critical points such as the F2, F1 and E layer peaks as anchor points to determine the electron density profile, using parameters of foF2, hmF2, foF1, hmF1, foE and hmE (the critical frequencies and peak heights of the F2, F1 and E layers, respectively) as inputs. As is well known, the F2 layer is the most important region of the ionosphere since the ionospheric electron density has its maximum values in this layer. Therefore, in empirical ionospheric models, hmF2 is one of the key parameters in the determination of the electron density profile. Although there are database of bottomside (such as the DIDBase, see Reinisch et al., 2004) and topside (such as the Alouette/ISIS topside sounder data, see Bilitza et al., 2006; Benson and Bilitza, 2009) electron density profiles providing hmF2 data, in practice, the value of hmF2 is usually calculated from the ionospheric propagation factor M(3000)F2 based on the strong anti-correlation existing between them (e.g., Bilitza, 1990), with a correction term related to the ratio of foF2/foE that accounts for the delay effect caused by ionizations in the E layer (Bradley and Dudeney, 1973; Bilitza et al., 1979). Usually, M(3000)F2 value is provided by the CCIR (International Radio Consultative Committee) M(3000)F2 model (CCIR Reports 340, 1967). However, some recent researches showed that CCIR-M(3000)F2 model has some remarkable discrepancies with observational data, in particular in the equatorial and low latitude regions (Adeniyi et al., 2003; Obrou et al., 2003; Zhang et al., 2004, 2007). Therefore, there is the necessity to update the existing M(3000)F2 model or

* Corresponding author. Fax: +86 10 62010846.
E-mail address: zhangml@mail.iggcas.ac.cn (M.-L. Zhang).

0273-1177/$36.00 © 2010 COSPAR. Published by Elsevier Ltd. All rights reserved.
doi:10.1016/j.asr.2010.06.004

construct directly a global model of hmF2. To achieve this goal, recently, some new modeling efforts have been made and modeling techniques have been proposed. For example, Oyeyemi et al. (2007) proposed a new modeling technique based on the application of neural network to model the M(3000)F2. Gulyaeva et al. (2008) derived a numerical model of hmF2 using topside sounding database of about 90,000 electron density profiles provided by satellite observations. Our team has been pursuing to develop another modeling technique based on empirical orthogonal function (EOF) decomposition to model the M(3000)F2 and hmF2 parameters (Liu et al., 2008; Zhang et al., 2009). First, a single station modeling technique based on EOF analysis has been developed and tested with good validity (Liu et al., 2008). Then the EOF based global modeling technique to model M(3000)F2 and hmF2 parameters has been developed (Liu et al., 2008; Zhang et al., 2009). The single station modeling technique is a fundamental part of our global modeling since it is used as means to fill single station data gaps for data-preprocessing in our global modeling development (Liu et al., 2008; Zhang et al., 2009). In this paper, we aim at evaluating of the global modeling technique based on three alternative EOF expansion methods of M(3000)F2 and hmF2 dataset. In Section 2, we will first describe briefly the modeling technique base on the three EOF expansion methods and the data used in the modeling and validating study. In Section 3 we will show some sample modeling results. The last section (Section 4) is the summary and conclusion.

2. Modeling technique description and data used for the modeling and validating study

The modeling technique we used is mainly based on the empirical orthogonal function (EOF) decomposition of a dataset. This method was first introduced into ionospheric empirical modeling by Dvinskikh (1988) and his work was followed by many others (e.g., Singer and Taubenheim, 1990; Bossy and Rawer, 1990; Singer and Dvinskikh, 1991; Dvinskikh and Naidenova, 1991). It has also been shown by many other researches that the EOF analysis is a powerful method in ionospheric data representation and empirical modeling (e.g., Daniell et al., 1995; Marsh et al., 2004; Matsuo et al., 2002, 2005; Mao et al., 2005, 2008; Materassi and Mitchell, 2005; Zhao et al., 2005; Zapfe et al., 2006; Liu et al., 2008; Zhang et al., 2009; and many more). The main point of this method is that it decomposes a dataset into a series of eigen function (or base functions) E_k and its associated coefficients A_k, with the base functions E_k orthogonal to each other. A very important feature of the EOF decomposition is that the eigen series converges very quickly. This makes it possible to use only a few orders of EOF components to represent most of the variance of the original dataset.

For details of our global modeling technique, please refer to Liu et al. (2008) and Zhang et al. (2009). Here we only give a brief description.

2.1. EOF decomposition of dataset

In our modeling study, the first step is to decompose the dataset using the EOF expansion. The EOF decompositions of a database can be made in any one of the following three ways. In the first decomposition method, the base functions E_k describe the variation of the dataset Y (Y can be either M(3000)F2 or hmF2) with the geographical latitude ($Glat$), longitude ($Glon$) and the universal time (UT), whereas the coefficients A_k represent the variation of the dataset with seasons (m) and solar cycle activity (represented by F107, the monthly mean solar irradiance flux index at the wavelength of 10.7 cm).

$$Y(Glon, Glat, UT, m, \mathrm{F107}) = \sum_{k=1}^{N} A_k(m, \mathrm{F107}) \cdot E_k(Glon, Glat, UT) \quad (1)$$

In the second decomposition method, the base function E_k describe the variation behavior of the dataset with the modified dip latitude (or modip, μ) and local time (LT) as well as the universal time (UT). The coefficients A_k represent the variation of the dataset with seasons and solar cycle activity.

$$Y(\mu, LT, UT, m, \mathrm{F107}) = \sum_{k=1}^{N} A_k(m, \mathrm{F107}) \cdot E_k(\mu, LT, UT) \quad (2)$$

In the third decomposition method, there are two layers of EOF decomposition. In the first layer, the dataset is decomposed into the EOF base functions E_k representing the variation of the dataset with the modified dip latitude (μ) and the local time (LT), and the associated EOF coefficients P_k representing the variations of the dataset with the universal time (UT) and seasonal as well as solar cycle variations as follows

$$Y(\mu, LT, UT, m, \mathrm{F107}) = \sum_{k=1}^{N} E_k(\mu, LT) \cdot P_k(UT, m, \mathrm{F107}) \quad (3)$$

Then the EOF coefficients P_k obtained in the first layer EOF analysis are decomposed once again into a series of base function F_k^j representing the variation with the universal time (UT) and the associated coefficients A_k^j representing the seasonal as well as solar cycle variations

$$P_k(UT, m, \mathrm{F107}) = \sum_{j=1}^{N1} F_k^j(UT) \cdot A_k^j(m, \mathrm{F107}) \quad (4)$$

Later on in this paper (Section 3), we will present the statistical analysis results (in Tables 1 and 2) on the model-data comparison for all these three alternative decomposition methods. However, we will only show those plots of the results obtained by applying the third EOF decomposition method to the dataset. Since we will show later, all the modeling with these three alternative decomposition methods have almost the same accuracy. However, from the point

Table 1
Regression correlation coefficients (R) between model and observational data for various models.

	R for M(3000)F2				R for hmF2			
	Model A	Model B	Model C	IRI	Model A	Model B	Model C	IRI
1965	0.904	0.905	0.909	0.841	0.949	0.950	0.948	0.862
1970	0.928	0.929	0.928	0.862	0.958	0.959	0.962	0.842

Table 2
Root-mean-squared-error ($RMSE$) between model and observational data for various models.

	$RMSE$ for M(3000)F2				$RMSE$ for hmF2 (km)			
	Model A	Model B	Model C	IRI	Model A	Model B	Model C	IRI
1965	0.09	0.09	0.09	0.12	11.2	11.2	11.8	18.9
1970	0.08	0.08	0.08	0.11	13.4	13.3	13.4	22.6

of view of simplicity and concise, the base functions $E_k(\mu, LT)$ and F_k^j in the third decomposition method are in the simplest format and easy to be presented in plots. It also requires much less storage space for its base function database and the associated EOF coefficients.

Hereafter, we will call models with the first, second and third decomposition methods as Model A, B and C.

2.2. Modeling the associated EOF coefficients A_k

The second step in our modeling is to model the EOF coefficients A_k with the following harmonic functions representing the seasonal (annual and semi-annual) and solar cycle variations.

$$A_k(m,\mathrm{F107}) = B_{k1}(m,\mathrm{F107}) + B_{k2}(m,\mathrm{F107}) + B_{k3}(m,\mathrm{F107}) \quad (5)$$

$$B_{k1}(m,\mathrm{F107}) = c_{k1} + d_{k1}\mathrm{F107} \quad (6)$$

$$B_{k2}(m,\mathrm{F107}) = (c_{k2} + d_{k2}\mathrm{F107})\cos\frac{2\pi m}{12} + (s_{k2} + t_{k2}\mathrm{F107})\sin\frac{2\pi m}{12} \quad (7)$$

$$B_{k3}(m,\mathrm{F107}) = (c_{k3} + d_{k3}\mathrm{F107})\cos\frac{2\pi m}{6} + (s_{k3} + t_{k3}\mathrm{F107})\sin\frac{2\pi m}{6} \quad (8)$$

where m is the month representing the seasonal variation, and F107 is the monthly mean solar irradiance flux index at the wavelength of 10.7 cm, a proxy used to represent the solar activity levels. With these equations, the coefficients $c_{k1}, d_{k1}, c_{k2}, d_{k2}, s_{k2}, t_{k2}, c_{k3}, d_{k3}, s_{k3}, t_{k3}$ are determined by the least-square fitting approaches.

Our model constructions are then made in the reversal procedure based on the obtained EOF base functions E_k (and F_k^j if the third decomposition method is used) as well as the coefficients $c_{k1}, d_{k1}, c_{k2}, d_{k2}, s_{k2}, t_{k2}, c_{k3}, d_{k3}, s_{k3}, t_{k3}$ obtained. Specifically, to calculate the model value of M(3000)F2 or hmF2, one first uses Eqs. (5)–(8), with the given month m and the corresponding solar flux index F107(m), to calculate the modeled second layer EOF coefficients A_k. Then, with the calculated modeled coefficients A_k, depending on the decomposition method used, Eq. (1) or Eq. (2) or Eqs. (3) and (4) are used to calculate the modeled value of Y (Y is either M(3000)F2 or hmF2).

2.3. Data used

For this study, measured monthly median hourly values of M(3000)F2 for the period of the years 1975–1985 from the ionosonde/digisonde stations distributed around the world were used for the M(3000)F2 global modeling study. The hmF2 data of the same period used for the modeling study is calculated from the measured M(3000)F2 based on the strong anti-correlation existing between them using formulae (Bilitza, 1990),

$$\mathrm{hmF2} = \frac{1490}{\mathrm{M(3000)F2} + \Delta M} - 176 \quad (9a)$$

$$\Delta M = \frac{F_1(R_{12})\cdot F_2(R_{12},\Phi)}{\mathrm{foF2/foE} - F_3(R_{12})} + F_4(R_{12}) \quad (9b)$$

$$F_1(R_{12}) = 0.00232\cdot R_{12} + 0.222 \quad (9c)$$

$$F_2(R_{12},\Phi) = 1 - R_{12}/150\cdot\exp(-\Phi^2/1600) \quad (9d)$$

$$F_3(R_{12}) = 1.2 - 0.0116\cdot\exp(R_{12}/41.84) \quad (9e)$$

$$F_4(R_{12}) = 0.096\cdot(R_{12} - 25)/150 \quad (9f)$$

where R_{12} is the 12-month running mean of the sunspot number, Φ is the magnetic dip latitude which is related to the magnetic inclination I as $2tg\Phi = tgI$. The measured M(3000)F2, foF2, foE used in calculation of hmF2 in this study were downloaded from Space Physics Interactive Data Resource (SPIDR) website http://spidr.ngdc.noaa.gov/. Fig. 1 shows the global distribution of the stations used for the M(3000)F2/hmF2 global modeling study. The total number of stations is about 86. There are still gaps in the coverage of the globe in the data used for this study. This data gap problem is overcome by a data-preprocessing procedure before applying the EOF expansion to the dataset. Procedure and details of data-preprocessing for the global modeling is described in Liu et al. (2008) and Zhang et al. (2009).

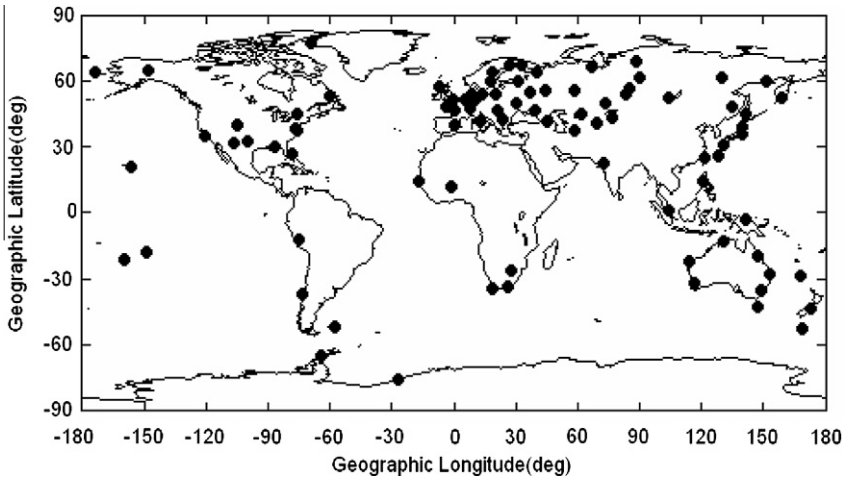

Fig. 1. Global distribution of the stations used for the present modeling study.

For evaluating the models' validity, data of M(3000)F2 and hmF2 for a low solar activity year (1965) and a high solar activity year (1970) are used to validate the models' performance. They are independent data from that used in model development.

3. Modeling results

To demonstrate the success of the modeling technique, here as an example, we show some sample plots (Figs. 2 and 3) obtained by applying the third EOF decomposition method to the dataset of M(3000)F2. The corresponding EOF expansion results for the hmF2 parameter are presented and discussed in Zhang et al. (2009), readers who are interested in may refer to that paper. Fig. 2 shows the contour plots of the first four orders of the base functions E_1–E_4 obtained with the 1st layer EOF decomposition. It can be seen that, apparently, the base functions E_k we obtained showed some typical features of M(3000)F2. For example, the 1st order of base function E_1 manifests mainly a typical phenomenon produced due to the 'fountain effect' in the equatorial ionosphere, whereas the 2nd base function

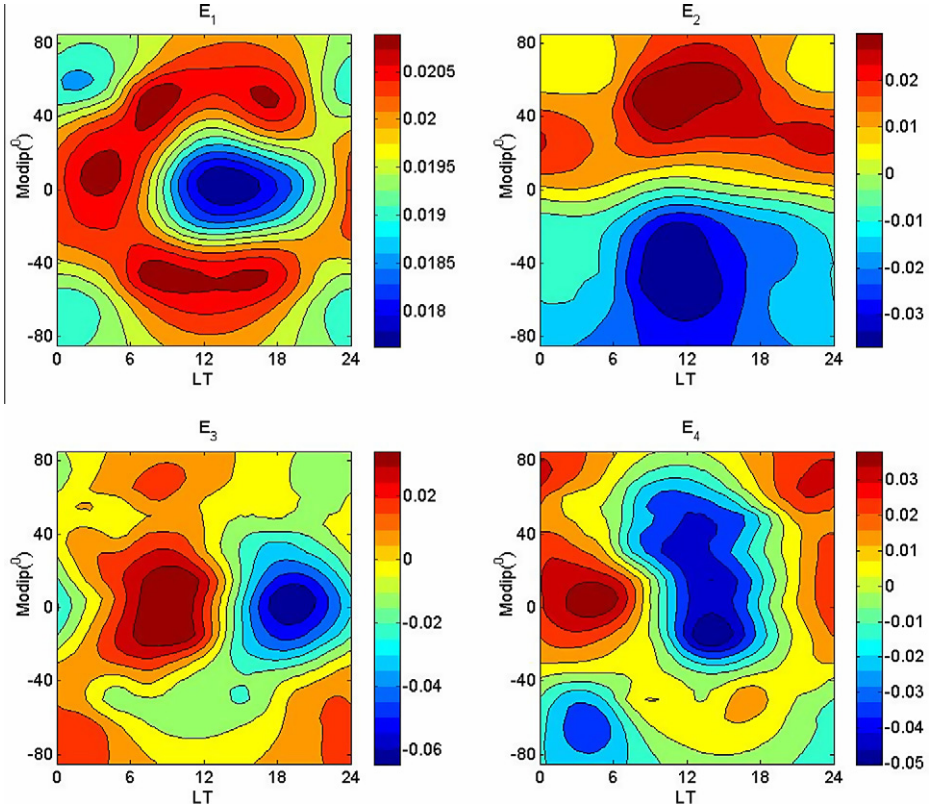

Fig. 2. Distribution of the first 4 base functions E_1–E_4 obtained with the 1st layer EOF decomposition of M(3000)F2.

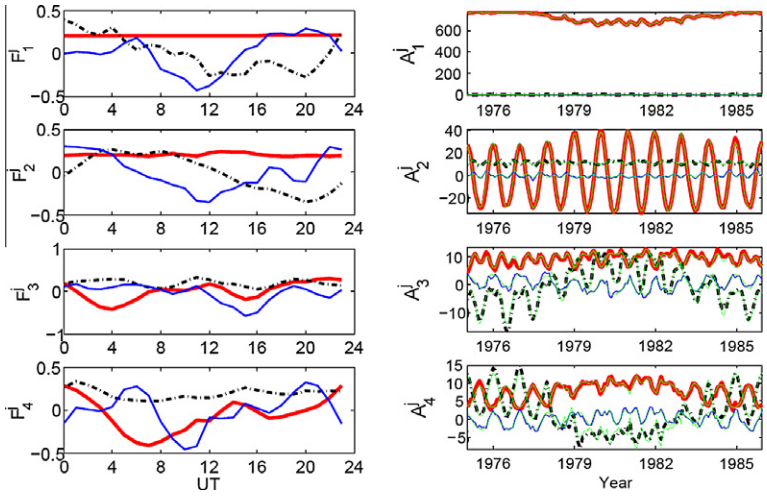

Fig. 3. Distribution of the EOF base functions $F_1^j - F_4^j$ (left panels) and their associated coefficients $A_1^j - A_4^j$ (right panels) obtained with the 2nd layer EOF decomposition of M(3000)F2. The three curves in each panel represent $j = 1$ (red), 2 (black), 3 (blue). The overlaying green lines in the right panels are the corresponding modeled results. (For interpretation of the references to color in this figure legend, the reader is referred to the web version of this article.)

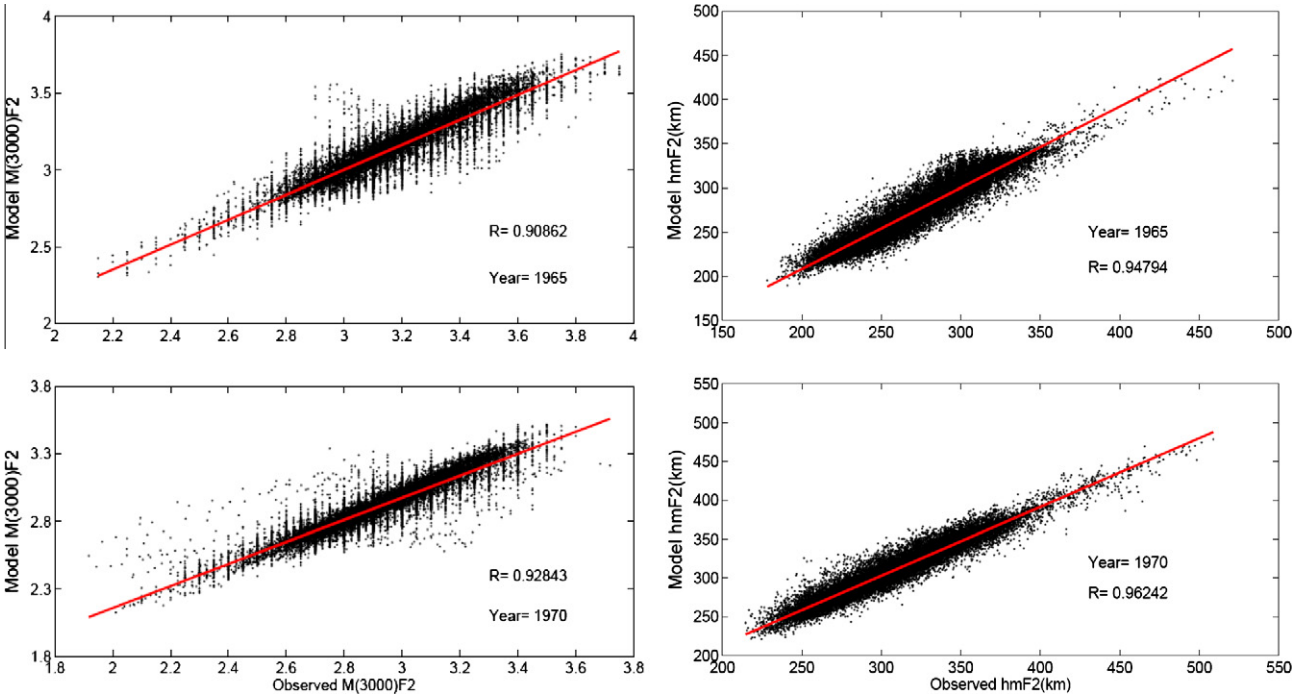

Fig. 4. Scatter plots of model value versus observational data for M(3000)F2 (left panels) and hmF2 (right panels).

E_2 mainly reflects the north-south asymmetry which is closely related to the seasonal change of the solar zenith angle. Therefore, the EOF decomposition analysis method, to some extent, is able to separate the variance of a dataset into components caused by sources due to different physical processes or mechanisms.

Fig. 3 shows the results obtained in the 2nd layer EOF analysis, that is, the EOF decomposition of P_k (see Eq. (4)). The left panels are the distributions of the base functions $F_1^j - F_4^j$ obtained, the right panels are for the corresponding associated coefficients $A_1^j - A_4^j$. The three lines in each panel represent $j = 1$ (red), 2 (black), 3 (blue). As we can see from the right panels, the 2nd layer EOF coefficients A_k^j mainly contains the annual and semiannual variation components and their amplitudes also change with the solar cycle activity levels. This justify the modeling of the coefficients A_k^j with the harmonic functions representing the seasonal (annual and semi-annual) variations as well as their solar cycle activity dependence represented by the F10.7 index as expressed by Eqs. (5)–(8). The overlaying green

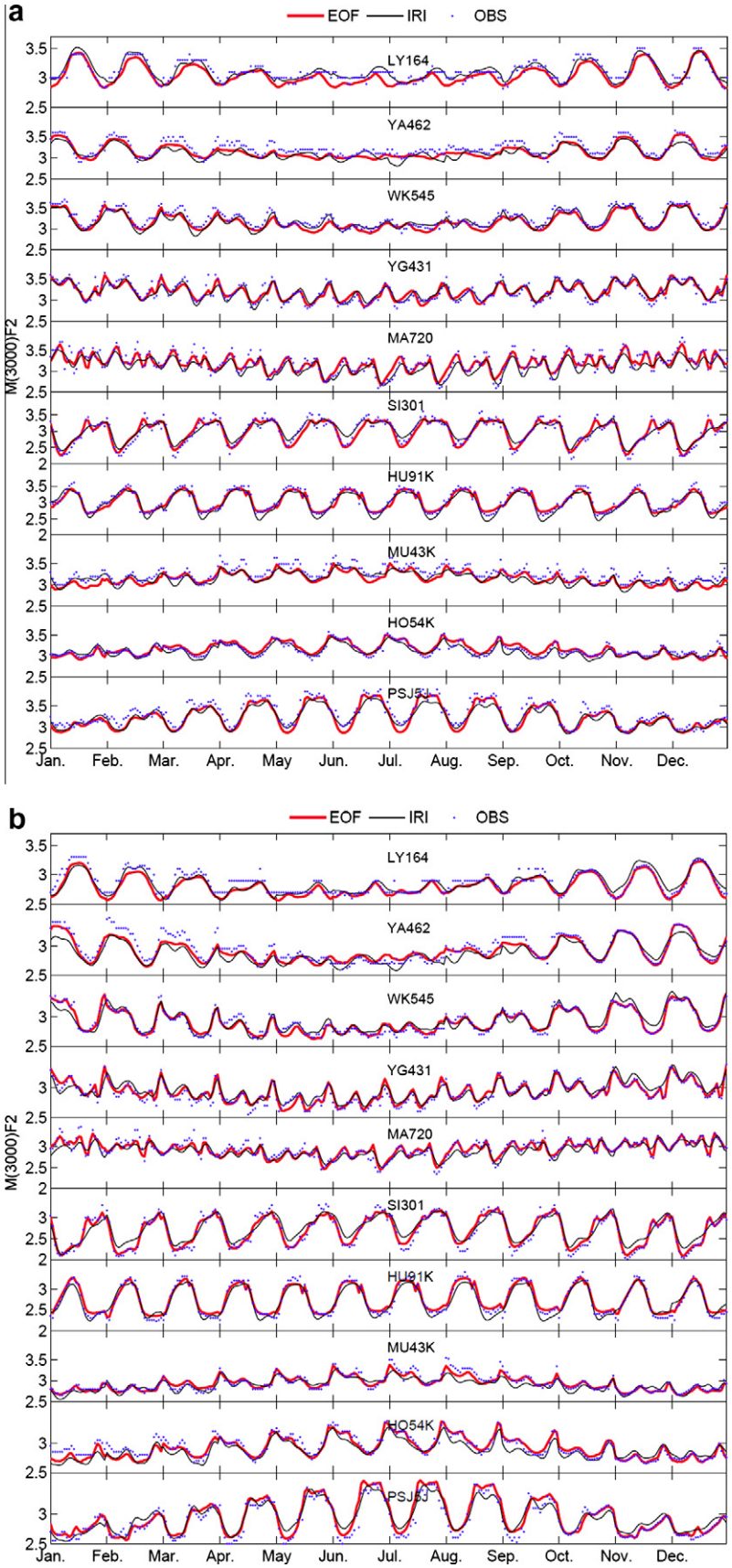

Fig. 5. Sample plots of model value and the observational data comparison for M(3000)F2 for the years of (a) 1965 and (b) 1970. (Blue dots, observational data; red thick values, EOF model; black thin curves, CCIR model.) (For interpretation of the references to color in this figure legend, the reader is referred to the web version of this article.)

lines in the right panels are the corresponding results modeled with Eqs. (5)–(8). As can be seen, the EOF coefficients A_k^j were reproduced very well by the modeled results.

Fig. 4 shows the scatter plots of the model value versus observational data for M(3000)F2 (left panels) and hmF2 (right panels). The upper panels are for the case of the low solar activity year (1965) and the lower panels for the case of the high solar activity year (1970). These two years data are independent of those used in modeling. It can be seen that the model values calculated with our constructed model based on the EOF decomposition and the observational data show a high linearity and the correlation coefficients R between the model values and the observational data are very high (for M(3000)F2, R is 0.91 and 0.93, and for hmF2, R is 0.95 and 0.96, respectively, for the years of 1965 and 1970). The high linearity and correlation coefficients between the modeled values and the observational data imply that the constructed model is able to reproduce the observational data quite well.

Fig. 5a and b show some sample plots demonstrating the comparison between the observational data of M(3000)F2 and the model values given by our EOF based model (Model C) as well as by the IRI-CCIR model for the low solar activity year 1965 (Fig. 5a) and the high solar activity year 1970 (Fig. 5b) for 10 stations representative of high, middle and low latitudes from both north and south hemispheres. In these plots, the red thick curves represent our EOF model results, the thin black curves represent the results given by IRI-CCIR model, and the blue points are the observational data. As can be seen from these plots, the EOF model results in general reproduced quite well the behavior of the observational data. Compared with the results given by IRI-CCIR M(3000)F2 model, the EOF model results are obviously in better agreement than the IRI-CCIR model results with the observational data. Similar comparisons with same conclusion have also been made for hmF2 parameter; interested readers may refer to Zhang et al. (2009) for details and plots showing the results. It has been pointed out that the IRI model cannot represent the sharp evening peak in hmF2 at magnetically low/equatorial latitudes that is due to the drift reversal (e.g., see Bilitza, 2003; Obrou et al., 2003). The CCIR spherical harmonics model is of too low order to be able to represent features smaller than the 1-hour level. Since our modeling uses monthly median hourly data of M(3000)F2 and hmF2, it would be expected that features smaller than 1-hour level could not be represented well in our EOF models. This problem can only be solved by using higher time resolution data (e.g., 15 min data) in the modeling when dataset of higher time resolution with enough long time period coverage (e.g., one solar clcye) are available. However, the EOF models we constructed do, to some extent, represent better the smaller scale features, as can be seen in the Fig. 5a and b in this paper and the Fig. 7a and b in Zhang et al. (2009).

Plots showing the comparison results for EOF based models using other decomposition methods (Model A and B) are not shown here for the sake of concise. Here we only list in Table 1 the regression correlation coefficients R between the EOF based models (with various decomposition methods) and the observational data. From Table 1, we can see that both for M(3000)F2 and hmF2, the correlation coefficients R between all three EOF based models and the observational data are similarly very high for both the low and high solar activity years, and that they are all much higher than that between the IRI model result and the observational data.

To estimate the accuracy of the constructed models, we made a statistical analysis on the differences between the model values and the observational data by calculating the root-mean-squared-error ($RMSE$):

$$RMSE = \sqrt{\frac{1}{N_p}\sum_{i=1}^{N_p}(Y_{model} - Y_{obs})^2} \tag{10}$$

where $Y =$ M(3000)F2 or $Y = hmF2$. Y_{model} denotes model value, Y_{obs} denotes observational data. N_p is the total number of the data points.

The calculated results of $RMSE$s for M(3000)F2 and hmF2 for the low solar activity year (1965) and the high solar activity year (1970) are shown in the Table 2. For the purpose of comparison, the $RMSE$s for IRI are also calculated and shown in the Table 2. As we can see in the Table 2, the $RMSE$s for the three models based on three alternative EOF expansion methods are more or less the same. Moreover, they are in general less than that of the IRI.

4. Summary and conclusion

In this study, global modeling techniques based on three alternative EOF expansion methods of the M(3000)F2 and hmF2 dataset are briefly described. Some sample plots showing the EOF decomposition results of M(3000)F2 dataset based on the third decomposition method are presented. Validating study of the constructed models based on all the three alternative EOF expansion methods are made using M(3000)F2 and hmF2 data that are independent of those used in model development. Comparisons between the model predictions and the observed data for both the low (1965) and the high (1970) solar activity years showed reasonably good agreement. Statistical analysis on the differences between model values and observed data showed that the constructed models based on all the three alternative EOF expansion methods have better agreement with the observed data than the models currently used in IRI. Statistically, all the three models based on the three alternative EOF expansions methods (Model A, B and C) showed very similar results, i.e., they have very similar accuracies. However, from the point of view of simplicity and concise, Model C is preferable. It requires much less storage space for its base function database and the associated EOF coefficients. It is also because the base functions E_k (μ, LT) in Model C is organized in the coordinate of

(μ, LT), a coordinate under which the features of the ionospheric parameters, in particular those of the F2 layer, are found mostly well organized (Rawer, 1963; Azpilicueta et al., 2006). Indeed, as we have demonstrated above and in Zhang et al. (2009), the EOF decomposition method used in Model C is able to separate the variance of a dataset into components caused by sources due to different physical processes or mechanisms.

Acknowledgments

This research was supported by the National Natural Science Foundation of China(40890164, 40774092), the National Important Basic Research Project (2006CB806306) and the China Meteorological Administration Grant (GYHY20070613). The M(3000)F2, foF2, foE and F107 index data used for the modeling study were downloaded from the SPIDR web site http://spidr.ngdc.noaa.gov/. The author M.-L. Zhang gratefully acknowledges the support of K.C. Wong Education Foundation, Hong Kong.

References

Adeniyi, J.O., Bilitza, D., Radicella, S.M., Willoughby, A.A. Equatorial F2-peak parameters in the IRI model. Adv. Space Res. 31 (3), 507–512, doi:10.1016/S0273-117703)00039-5, 2003.

Azpilicueta, F., Brunini, C., Radicella, S.M. Global ionospheric maps from GPS observations using modip latitude. Adv. Space Res. 38 (11), 2324–2331, doi:10.1016/jasr.2005.07.069, 2006.

Benson, R.F., Bilitza, D. New satellite mission with old data: rescuing a unique data set. Radio Sci. 44, RS0A04, doi:10.1029/2008RS004036, 2009.

Bilitza, D., Sheikh, N.M., Eyfrig, R. A global model for the height of the F2-peak using M3000 values from the CCIR numerical map. Telecommun. J. 46, 549–553, 1979.

Bilitza, D. International Reference Ionosphere 1990. Rep. NSSDC/WDC-R&S 90-22, World Data for Rockets and Satell., Nat. Space Sci. Data Cent., Greenbelt, Md., 1990.

Bilitza, D. International Reference Ionosphere 2000. Radio Sci. 36 (2), 261–275, doi:10.1029/2000RS002432, 2001.

Bilitza, D. International Reference Ionosphere 2000 – examples of improvements and new features. Adv. Space Res. 31 (3), 151–167, 2003.

Bilitza, D., Reinisch, B.W., Radicella, S.M., Pulinets, S., Gulyaeva, T., Triskova, L. Improvements of the International Reference Ionosphere model for the topside electron density profile. Radio Sci. 41 (RS5S15), 1–8, 2006.

Bossy, L., Rawer, K. Discussion of a new method for mapping ionospheric characteristics. Adv. Space Res. 10 (11), 65–74, doi:10.1016/0273-117790)90307-L, 1990.

Bradley, P.A., Dudeney, J.R. A simple model of the vertical distribution of electron concentration in the ionosphere. J. Atmos. Terr. Phys. 35, 2131–2146, 1973.

CCIR, Comite Consultatif International des Radiocommunications. Reports 340, 340-2 and later supplements, Geneva, 1967.

Daniell, R.E., Brown Jr., L.D., Anderson, D.N., Fox, M.W., Doherty, P.H., Decker, D.T., Sojka, J.J., Schunk, R.W. Parameterized ionospheric model: A global ionospheric parameterization based on first principles models. Radio Sci. 30 (5), 1499–1510, doi:10.1029/95RS01826, 1995.

Dvinskikh, N.I. Expansion of ionospheric characteristics fields in empirical orthogonal functions. Adv. Space Res. 8 (4), 179–187, doi:10.1016/0273-117788)90238-4, 1988.

Dvinskikh, N.I., Naidenova, N.Ya. An adaptable regional empirical ionospheric model. Adv. Space Res. 11 (10), 7–10, doi:10.1016/0273-117791)90312-8, 1991.

Gulyaeva, T.L., Bradley, P.A., Stanislawska, I., Juchnikowski, G. Towards a new reference model of hmF2 for IRI. Ads. Space Res. 42 (4), 666–672, doi:10.1016/j.asr.2008.02.021, 2008.

Leitinger, R., Zhang, M.L., Radicella, S.M. An improved bottomside for the ionospheric electron density model NeQuick. Ann. Geophys. 48 (3), 525–534, 2005.

Liu, C., Zhang, M.-L., Wan, W., Liu, L., Ning, B. Modeling M(3000)F2 based on empirical orthogonal function analysis method. Radio Sci. 43, RS1003, doi:10.1029/2007RS003694, 2008.

Mao, T., Wan, W., Liu, L. An EOF-based empirical model of TEC over Wuhan. Chin. J. Geophys. 48 (4), 751–758, 2005.

Mao, T., Wan, W., Yue, X., Sun, L., Zhao, B., Guo, J. An empirical orthogonal function model of total electron content over China. Radio Sci. 43, RS2009, doi:10.1029/2007RS003629, 2008.

Marsh, D.R., Solomon, S.C., Reynolds, A.E. Empirical model of nitric oxide in the lower thermosphere. J. Geophys. Res. 109, A07301, doi:10.1029/2003JA010199, 2004.

Materassi, M., Mitchell, C.N. A simulation study into constructing of the sample space for ionospheric imaging. J. Atmos. Sol. Terr. Phys. 67 (12), 1085–1091, doi:10.1016/j.jastp.2005.02.019, 2005.

Matsuo, T., Richmond, A.D., Nychka, D.W. Modes of high-latitude electric field variability derived from DE-2 measurements: Empirical Orthogonal Function (EOF) analysis. Geophys. Res. Lett. 29 (7), 1107, doi:10.1029/2001GL014077, 2002.

Matsuo, T., Richmond, A.D., Lu, G. Optimal interpolation analysis of high-latitude ionospheric electrodynamics using empirical orthogonal functions: estimation of dominant modes of variability and temporal scales of large-scale electric fields. J. Geophys. Res. 110, A06301, doi:10.1029/2004JA010531, 2005.

Obrou, O.K., Bilitza, D., Adeniyi, J.O., Radicella, S.M. Equatorial F2-layer peak height and correlation with vertical ion drift and M(3000)F2. Adv. Space Res. 31 (3), 513–520, doi:10.1016/S0273-117703)00024-3, 2003.

Oyeyemi, E.O., Mckinnell, L.A., Poole, A.W.V. Neural network-based prediction techniques for global modeling of M(3000)F2 ionospheric parameter. Adv. Space Res. 39 (5), 643–650, doi:10.1016/j.asr.2006.09.038, 2007.

Rawer, K., in: Landmark, B. (Ed.), Meteorological and Astronomical Influences on Radio Wave Propagation. Pergamon Press, Oxford, pp. 221–250, 1963.

Reinisch, B.W., Galkin, I.A., Khmyrov, G., Kozlov, A., Kitrosser, D.F. Automated collection and dissemination of ionospheric data from the digisonde network. Adv. Radio Sci. 2, 241–247, 2004.

Singer, W., Dvinskikh, N.I. Comparison of empirical models of ionospheric characteristics developed by means of different mapping methods. Adv. Space Res. 11 (10), 3–6, doi:10.1016/0273-117791)90311-7, 1991.

Singer, W., Taubenheim, J. Application of the expansion into empirical orthogonal functions to ionospheric characteristics. Adv. Space Res. 10 (11), 59–64, doi:10.1016/0273-117790)90306-K, 1990.

Zapfe, B.D., Materassi, M., Mitchell, C.N., Spalla, P. Imaging of the equatorial ionospheric anomaly over South America – a simulation study of total electron content. J. Atmos. Sol. Terr. Phys. 68 (16), 1819–1833, doi:10.1016/j.jastp.2006.05.025, 2006.

Zhang, M.L., Shi, J.K., Wang, X., Wu, S.Z., Zhang, S.R. Comparative study of ionospheric characteristic parameters obtained by DPS-4 digisonde with IRI2000 for low latitude station in China. Adv. Space Res. 33 (6), 869–873, doi:10.1016/j.asr.2003.07.013, 2004.

Zhang, M.L., Shi, J.K., Wang, X., Shang, S.P., Wu, S.Z. Ionospheric behavior of the F2 peak parameters foF2 and hmF2 at Hainan and comparisons with IRI model predictions. Adv. Space Res. 39 (5), 661–667, doi:10.1016/j.asr.2006.03.047, 2007.

Zhang, M.-L., Liu, C., Wan, W., Liu, L., Ning, B. A global model of the ionospheric F2 peak height based on EOF analysis. Ann. Geophys. 27 (8), 3203–3212, 2009.

Zhao, B., Wan, W., Liu, L., Yue, X., Venkatraman, S. Statistical characteristics of the total ion density in the topside ionosphere during the period 1996–2004 using empirical orthogonal function (EOF) analysis. Ann. Geophys. 23, 3615–3631, 2005.